Current Topics

AFM: A Nanotool in Membrane Biology[†]

Daniel J. Muller*

Biotechnology Center, Technische Universität Dresden, D-01307 Dresden, Germany

Received April 28, 2008; Revised Manuscript Received June 15, 2008

ABSTRACT: Cellular membranes are vital for life. They confine cells and cytosolic compartments and are involved in virtually every cellular process. Cellular membranes form cellular contacts and focal adhesions, anchor the cytoskeleton, generate energy gradients, transform energy, transduce signals, move cells, and actively form compartments to assemble different membrane proteins into functional entities. But how do cellular membranes perform these tasks? What do the machineries of cellular membranes look like, and how are they controlled and guided? Atomic force microscopy (AFM) allows the observation of biological surfaces in their native environment at a signal-to-noise ratio superior to that of any optical microscopic technique. With a spatial resolution approaching ≈1 nm, AFM can identify the supramolecular assemblies, characteristic structure, and functional conformation of native membrane proteins. In recent years, AFM has evolved from imaging applications to a multifunctional "laboratory on a tip" that allows observation and manipulation of the machineries of cellular membranes. In the force spectroscopy mode, AFM detects interactions between two single cells at molecular resolution. Force spectroscopy can also be used to probe the local elasticity, chemical groups, and receptor sites of live cells. Other applications locate molecular interactions driving membrane protein folding, assembly, and their switching between functional states. It is also possible to examine the energy landscape of biomolecular reactions, as well as reaction pathways, associated lifetimes, and free energy. In this review, we provide a flavor of the fascinating opportunities offered by the use of AFM as a nanobiotechnological tool in modern membrane biology.

Membranes define the cell boundary and surround the various cellular compartments. Such compartmentalization has been essential for the development of life and reflects an important multifunctional tool of organisms. The function and structure of cellular membranes are diverse and specific to individual organisms and tissues and dynamically adapt to the environmental and functional state of the cell. Cellular membranes must take up nutrients, small molecules, and ions, release waste products, bind ligands, transmit signals, convert energy, sense the environment, maintain cell adhesion, control cell migration, and much more while forming a tight barrier. To be able to provide such functions, cellular membranes consist of many different molecular components. These small molecules and macromolecules such as lipids, cholosterol, carbohydrates, and membrane proteins are asymmetrically distributed over the cellular membrane forming functional compartments (*1*). In many cells, this functional "patchiness" of cellular membranes is dynamically remodeled to fulfill specific tasks.

Given the biological importance of cellular membranes, their complexity has been surprisingly neglected by biochemists and cell biologists until recently. This is understandable in spite of a lack of technical possibilities for visualizing and characterizing these complex machineries of the cell. Different microscopy approaches to characterizing cellular membranes have been developed. Most of them are based on either light or electron microscopy. Recent developments in optical methods allow revealing nanoscopic images of fluorescently labeled biological objects (*2*) and electron microscopy tomographs providing molecular insights into vitrified cells (*3*). Here, we introduce atomic force microscopy (AFM) as a complementary microscopy technique that allows the imaging of cellular membranes at a spatial resolution down to 1 nm. Most importantly to biologists, AFM images biological specimens in buffer solutions, at ambient temperatures, and without the need for fixation, staining, or labeling. The signal-to-noise (*S*/*N*) ratio of the atomic force microscope is superior to that of any optical or electron microscope and allows the observation of single membrane proteins peppering a cellular membrane. Moreover, the AFM probe originally invented to contour the topography of an object has developed into a multifunctional nanotool. Functionalization converts the AFM probe into a "laboratory on a tip" that, for example, can detect, while scanning cellular membranes, many different biophysical and chemical variables (*4, 5*). Using this multifunctional approach, it has became possible to directly correlate structural information with functional information. In this paper, we will give an overview of AFM and its exciting applications in membrane biology.

[†] This work was supported in part by the Deutsche Forschungsgemeinschaft (DFG), the European Union, and the Free State of Saxony.

* To whom correspondence should be addressed. E-mail: mueller@biotec.tu-dresden.de. Telephone: +49-351-46340330. Fax: +49-351-46340342.

10.1021/bi800753x CCC: $40.75
Published on Web 07/11/2008

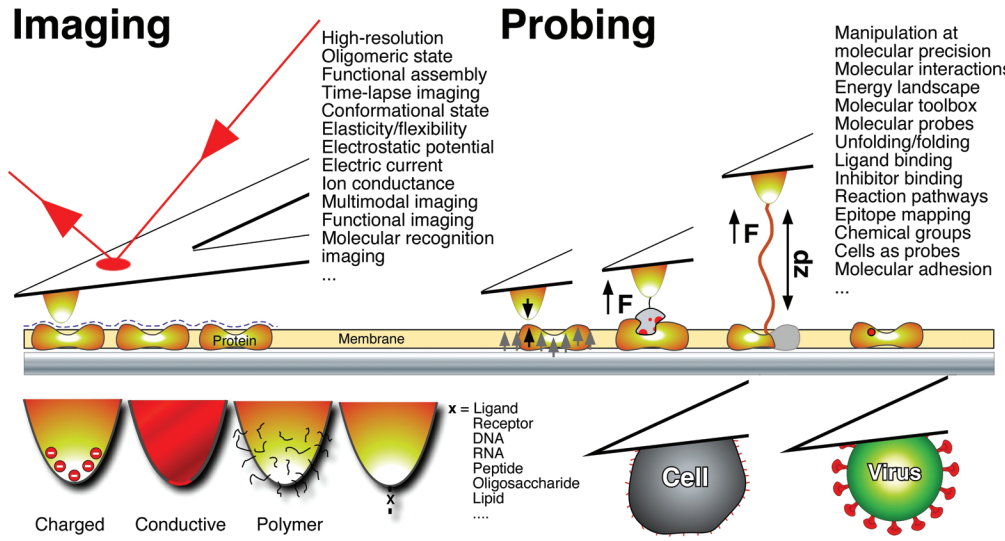

FIGURE 1: AFM-based nanotools provide a laboratory on a tip for imaging and probing biological membranes at the molecular level. The scanning probe technique, AFM, has greatly inspired nanobiotechnology and opened up a variety of unique possibilities for characterizing cells and their machineries. In the AFM imaging mode, the AFM probe is used to contour (blue dashed line) the topography of biological membranes under physiological conditions. The resolution can be sufficiently high to reveal individual membrane proteins and their substructures. Applications and imaging modes are listed at the right. For a detailed overview of AFM imaging modes, see ref *4*. Functional probes convert the AFM cantilever into a tool for detecting a plethora of biological, chemical, and physical interactions. Applications and probing modes are listed at the right. Selected examples developed to characterize biological objects using functionalized probes (not to scale) are illustrated in the top right and bottom panels. In the top right panel, the first example shows an atomic force microscope probing the local elasticity of a biological membrane. The AFM probe in the second example measures the interaction of a single receptor−ligand pair. The third example shows an AFM probe unfolding a membrane protein, and the fourth shows the site of ligand binding located by the AFM probe. In the bottom panel, from left to right, are shown a charged AFM probe for sensing electrostatic potentials, an AFM probe that is conductive only at its very tip for measuring local electric currents, and a polymer-coated probe for detecting interactions of the polymer. The x stands for functionalization of the AFM probe for the purpose of specifically attaching biological molecules. The functionalized probe can then characterize specific interactions of these molecules. Other approaches attach a living cell or a virus to the AFM cantilever to detect cellular or viral interactions.

AFM: Imaging and Probing The principle of AFM (*4*) is comparable to a blind persons use of a stick to probe the environment. The atomic force microscope has a microscopic cantilever, analogous to the stick, the apex of which has a molecularly sharp probe. To reveal the topography of a biological object, the probe is raster scanned over the object while the cantilever deflection at every pixel is measured (Figure 1). When scanning over an uneven surface, the cantilever bends, and a piezo actuator moves the cantilever (or sample) vertically to keep the forces applied by the probe to the object constant. The height value for each scanned pixel reveals the topography of the object. However, the forces between the probe and object can have manifold inter- and intramolecular interactions as origins. Consequently, procedures have been established that functionalize the AFM probe and allow it to selectively sense certain interactions among these. On the basis of this principle to specifically probe one out of a variety of possible interactions at molecular precision, many AFM-based scanning probe microscopes (SPM) have been developed. This simple adaptation has converted AFM into a multifunctional tool, or a laboratory on a tip, which has sparked the nanotechnology revolution (*4*), and a similar revolution is foreseen in biology.

In the near future, atomic force microscopes will be commercially available for imaging biological specimens at molecular resolution and equipped with multifunctional probes that allow detailed analyses of biological objects (*4, 5*). However, AFM imaging, as a surface sensitive technique, is currently limited to the characterization of surfaces. Flat and smooth samples, such as cell membranes, are exceptionally well suited to characterization by AFM-based probes. Thus, AFM-based technologies are particularly versatile when applied in membrane biology. Surprisingly, AFM probing can also take a look inside membranes, and the experiments have examined folding, interactions, and functional states of membrane proteins.

Advantage of Single-Molecule Experiments. AFM offers great potential for characterizing single molecules and thus offers many advantages in scientific discoveries. Contrary to detection of an ensemble of events as in bulk experiments, single-molecule experiments directly measure individual molecular properties. Consequently, single-molecule experiments capture transient intermediates in a biochemical process, which previously could be accomplished only by synchronizing the actions of a large ensemble of molecules. Examples of such experiments, discussed in this review, are those with heterogeneous structural intermediates detected during membrane protein unfolding. These examples show the coexistence of multiple unfolding pathways and reaction pathways. Other examples discuss coexisting conformational states of single-membrane proteins. Here, the single-molecule trajectories provide insights into the dynamic population shift of intermediates and pathways. Such trajectories provide detailed information about reaction steps and kinetics, which is unavailable from traditional ensemble experiments. These advances provided by single-molecule experiments provide not only new opportunities for deciphering protein dynamics but also significant challenges, ranging from experimental and theoretical to statistical. The statistical challenges arise from the stochastic nature of single-molecule trajectories. Whereas the experimental and theoretical issues have been addressed considerably, the statistical aspects

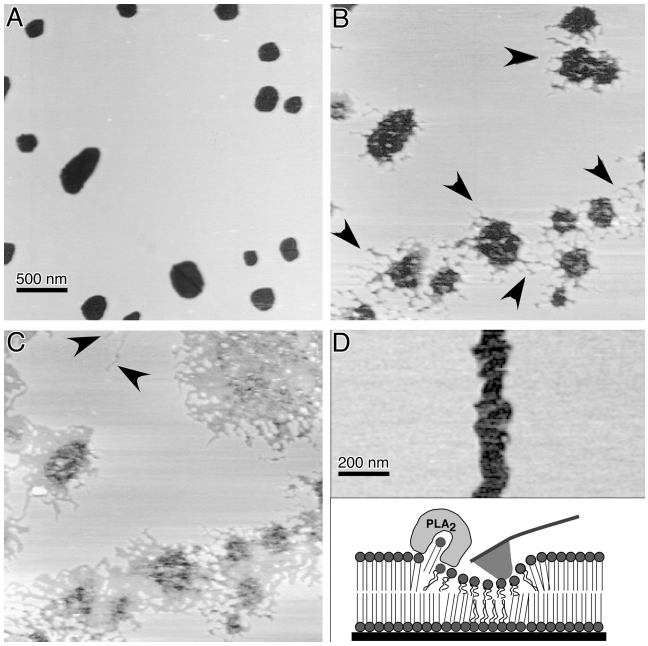

FIGURE 2: Time-lapse AFM depicts the remodeling of a DPPC bilayer by phospholipase A_2. (A) DPPC bilayer imaged in buffer solution before addition of PLA_2. Dark holes are defects in the supported bilayer. (B) Addition of PLA_2 induces remodeling of the lipid bilayer. Arrows point out small channels that are indicative of phospholipid hydrolysis by PLA_2. (C) With increasing time (4 min), the phospholipid bilayer becomes increasingly hydrolyzed. (D) Scanning the DPPC bilayer while applying a strong force (2 nN) to the AFM probe induces small perturbations that provide PLA_2 a possibility for hydrolysis along the scanned line (topography and illustration). Images courtesy of H. E. Gaub and H. Clausen-Schaumann (*6*). Reproduction permission kindly provided by *Biophysical Journal*. Copyright 1998 Biophysical Society.

of single-molecule studies demand significant attention and improvement.

Watching Enzymes and Polypeptides Remodeling Membranes. The study of membrane biology includes characterizing how enzymes, polypeptides, and membrane proteins interact with lipid membranes. In 1998, the Gaub group (*6*) applied time-lapse AFM to directly observe phospholipase A_2 (PLA_2) degrading dipalmitoylphosphatidylcholine (DPPC) bilayers (Figure 2). The degradation creates channels as small as the width of a single enzyme. The PLA_2 activity depended on the phospholipid organization and orientation within the bilayer and was enhanced by defects in the bilayer. These findings inspired researchers to use the AFM probe to mechanically perturb the bilayer and determine the enzymatic activity of PLA_2. Similar AFM-based approaches were used to characterize the activity, kinetics, and mechanisms of lipases remodeling supported lipid bilayers (*7, 8*), the solubilization of phospholipid bilayers by amphiphiles (*9*) or acylated C_{14}-peptides (*10*), and the remodeling of lysosomal membranes by saposin (*11*). The remodeling of lipid membranes by saposin C was shown to provide acid glucosidase (GCase) access to its membrane-embedded glycosphingolipid substrate and to hydrolyze glucose from glucosylceramide (*11*).

In 2000, the de Kruijff group visualized the remodeling of phosphatidylcholine (PC) bilayers by transmembrane α-helices forming WALP polypeptides (*12*). Striated lateral domains formed in DPPC bilayers. These assembled into well-ordered hexagonal patterns exhibiting lateral distances of 8 nm (see the example given in Figure 8A). This pattern was independent of the WALP polypeptide length in the range from 2.5 to 4.2 nm. The reorganization of lipid bilayers into domains was also characterized in the presence of sphingolipid ceramide (*13*). Others have visualized the remodeling of ordered phosphatidylcholine membrane microscopic domains by inserting the glycosylphosphatidylinositol (GPI)-anchored intestinal alkaline phosphatase (BIAP) from bovine (*14*). AFM topographs reporting the remodeling of the lipid bilayers do not reveal individual enzymes attached to the membrane or membrane proteins. One of the reasons is that although most of the topographs exhibit a high vertical resolution of ≈0.2 nm the lateral resolution is only ≈10 nm. Such a "low" resolution does not allow structural identification of specific membrane proteins. However, this changes as a high spatial resolution of ≈1 nm is approached.

High-Resolution Imaging of Native Transmembrane Proteins and Membranes. Being a prerequisite for revealing high-resolution AFM topographs of transmembrane proteins, procedures for sample preparation (*15, 16*) and imaging (*17*) have been established and described well. To identify the sidedness of membrane proteins, several procedures have been established. One must consider that in contrast to electron or optical microscopy the combination of exceptionally high resolution and *S*/*N* ratio allows AFM to directly observe single antibodies. Immuno-AFM uses this advantage to watch individual antibodies specifically binding to their target and, thus, to identify the sidedness of membrane proteins (*18*). After imaging, the AFM probe can be used as a nanoscopic tweezer to remove the attached antibodies and to structurally identify the membrane protein. Other approaches identify the sidedness of membrane proteins by comparing high-resolution topographs recorded before and after enzymatic removal of polypeptide loops and terminal ends (*19, 20*). Alternatively, changes in the size of polypeptide loops engineered into the protein can also be used (*21*).

AFM topographs with spatial resolutions of ≈1 nm allow single membrane proteins to be observed and reveal details of their surface structures (Figure 3) (*17, 22*). However, the force applied during the imaging process must be carefully balanced to contour the native protein surface while preventing reversible and irreversible structural deformations (*22*). To develop reproducible protocols for the recording of high-resolution AFM topographs of native proteins, the Engel group systematically investigated the contrast mechanism of AFM topographs that have been recorded (*22*). This was complicated because different kinds of forces act between the AFM probe and the protein. For example, the topographic height differences measured by AFM can show significant electrostatic contributions (*23, 24*). In most cases, the electrostatic contributions extending over long interaction distances of ≫1 nm do not contribute to the imaging of native proteins, whereas short-range interactions of <1 nm do (*17*). On the basis of these insights, high-resolution imaging procedures that adjust long-range electrostatic forces interacting between the probe and the substructures of the protein were developed (*17*). Currently, the AFM imaging procedures allow the contouring of polypeptide loops that are only a few amino acids in size (*22, 25*).

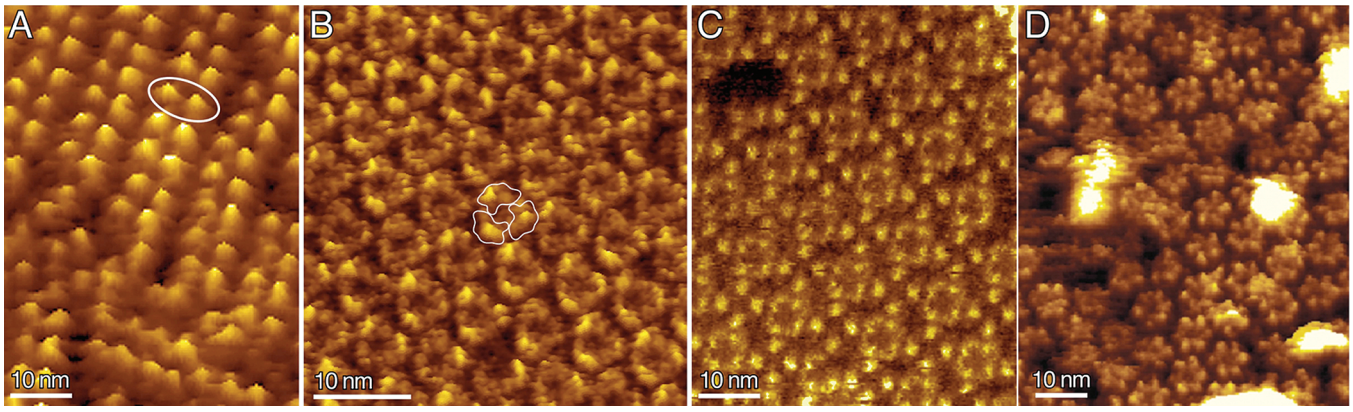

FIGURE 3: Observing the oligomeric states of vertebrate and bacterial rhodopsins. (A) Rhodopsin from the disk membrane of the rod outer segment of the bovine eye (*40*). The ellipse denotes two protrusions of rhodopsin molecules forming a dimer. (B) Cytoplasmic surface of the native purple membrane from *Halobacterium salinarum* (*28*). Individual bacteriorhodopsin molecules form trimers (outline) that assemble into a two-dimensional hexagonal lattice. Substructures of bacteriorhodopsin molecules denote their cytoplasmic polypeptide loops. (C) Tetrameric assembly of halorhodopsin molecules from *H. salinarum* (*42*). (D) Proteorhodopsin molecules from planktonic bacteria can assemble into pentamers and hexamers (*43*). All topographs were recorded in buffer solution at room temperature using contact mode AFM.

Observing the Structural Variability of Native Membrane Proteins. The imaging of single-membrane proteins and their substructures allows structural variations to be observed (*22, 26*). Apparently, certain structural regions exhibit a higher structural flexibility than others. This indicates that heterogeneous mechanical properties occur within membrane proteins. It has been suggested that such differences in mechanical properties contribute to functional conformations of membrane proteins (*27*). In another experiment, AFM was used to probe the flexibility of the surface structures of the light-driven proton pump bacteriorhodopsin. It was observed that the polypeptide loop connecting transmembrane α-helices E and F of bacteriorhodopsin exhibited high flexibility (*22, 28*). The flexibility of this loop is thought to be important for function, as helix F tilts during the photocycle. The ability to distinguish individual conformations of flexible domains of membrane proteins allows the classification of these conformations (*26*). This is extended to calculating the probabilities and entropies of membrane protein conformations. Such mechanical and energetic insights can contribute significantly to our understanding of the functional mechanisms of membrane proteins (*29, 30*). In the future, the analysis of conformational flexibilities, classes, and probabilities may reveal how physiological parameters influence membrane protein conformations. Such parameters include the lipid composition of the membrane, the binding of a ligand or inhibitor, the oligomerization, the supramolecular assembly, and the functional state of the protein.

Controlled Dissection of Membranes and Membrane Proteins. In combination with topographical imaging, the AFM probe can be used as a tweezer that dissects membranes and membrane proteins. The first biological membrane dissected by AFM was a gap junction plaque isolated from a rat liver cell (*31*). After the gap junction plaque had been imaged, the force applied to the scanning AFM probe were increased until the upper membrane layer was swept away, after which the gap junction hemichannels from the underlying layer could be imaged (*27*). In another example, the AFM probe was used to dissect eye lens membranes adhering together via major intrinsic proteins (MIPs) (*32*).

A decade ago, Fotiadis et al. imaged the 340 kDa pigment-containing reaction center photosystem I (PSI) from the thermophilic cyanobacterium *Synechococcus* sp. at a lateral resolution of ≈2 nm (*33*). Repetitive scanning of the reconstituted PSI complex with the AFM probe removed individual proteins. Time-lapse AFM imaging of PSI before and after removal of subunits yielded structural insight into their interfaces. In another example, proteins attached to the photosynthetic core complexes in native *Rhodopseudomonas viridis* membranes (*34*) were dissected. These examples demonstrate that membranes as well as membrane proteins can be observed and manipulated at nanometer precision and that AFM is a unique nanotool.

Imaging the Oligomeric and Supramolecular Assembly of Membrane Proteins. AFM has frequently been used to observe the oligomeric assembly of membrane proteins. Examples include α-hemolysin (*35*), cholera toxin (*36*), ion-driven rotors of F_oF_1-ATP synthases from different organisms (*37–39*), and bovine rhodopsin (*40, 41*). Examples from different bacterial and vertebrate rhodopsins show that AFM topographs can have sufficiently high resolution to distinguish the individual proteins within the oligomers (Figure 3). Moreover, topographs recorded at an exceptionally high resolution of ≈0.5 nm revealed that the surface structures of a membrane protein could depend on its oligomeric state (*28*). Bacteriorhodopsins assembled in dimeric and trimeric forms arranged their individual polypeptide loops differently. This structural change was unexpected because bacteriorhodopsin, having evolved to function under harsh conditions, is an unusually robust membrane protein. Although speculative, this observation implies that the hetero- and homodimeric assemblies of other membrane proteins change their surface structures with their oligomeric states. Relevant examples in this regard are G-protein-coupled receptors (GPCRs). Homo- and heterodimeric assemblies of GPCRs modulate their functions differently (*41*), which includes interactions of the GPCR surface with G-proteins for signal transduction. High-resolution AFM could be a convenient approach to observing the extent to which the surface structures of individual GPCRs change with regard to oligomerization and functional states.

The assembly of membrane proteins is restructured depending on the functional state of the cell. Functionally related compartments are formed by the interplay of lipids,

membrane proteins, small molecules, and environmental parameters such as membrane tension, electrolyte, electrolyte concentration, temperature, and pH. AFM imaging of the photosynthetic membrane in the light- and dark-adapted state was the first experiment which could directly observe this assembly (*44*). It was found that the concentration of light-harvesting II (LH2) complexes was increased in the dark-adapted state, while the number of reaction centers collecting energy from surrounding LH2 complexes was increased in the light-adapted state. Other topographs showed in exceptional structural detail how individual reaction centers assemble within single-LH1 complexes (*34, 45*). AFM topographs of freshly isolated outer mitochondrial membranes revealed that voltage-dependent anion channels (VDAC) could assemble into monomers, tetramers, hexamers, and higher-order oligomers (*46*). This oligomeric heterogeneity supposedly modulates VDAC.

One must consider that via extraction of a membrane patch from the cell its native environment is modified. Frequently, the supramolecular arrangement of membrane proteins in functional compartments is a dynamic process that relies on various feedback mechanisms. The isolation of these membranes from the cell disrupts the mechanisms that regulate the location and assembly of membrane proteins. It is often challenging to show that the supramolecular assemblies imaged by AFM reflect the in vivo state. Therefore, a future goal is to characterize functional supramolecular assemblies of membrane proteins in cells or organelles.

Watching Membrane Proteins at Work. Understanding how membrane proteins function necessitates a grasp of the sequence of conformations that alter their functional states. To record a high-resolution topograph using commercially available atomic force microscopes takes ≈90 s. Most molecular biological processes occur on much faster time scales. Thus, imaging the conformations of different functional states of membrane proteins by the current AFM technology requires the proteins to be kinetically trapped in one state. Several conformational changes of native membrane proteins have been imaged by time-lapse AFM (*22, 27, 47–50*). Examples include the conformational change of a protein surface layer (S-layer) that covers *Deinoccocus radiodurans*. High-resolution AFM showed the plugged and unplugged conformations of S-layer pores to coexist. Time-lapse topographs revealed the switching of these pores between "open" (unplugged) and "closed" (plugged) conformations (*22, 47*). The outer membrane protein porin OmpF of *Escherichia coli* was shown to be gated by the electrostatic potential across the membrane. AFM topographs show that conformational changes of the large and flexible extracellular polypeptide loop of OmpF close the channel entrance (*48*). Later, this reversible closure was shown to occur in other outer membrane proteins of the same family (*51*). Topographs of gap junction plaques isolated from HeLa cells revealed the opening of single channels (*27*). After nanodissection of the upper membrane of the plaque, the extracellular surface of the Cx26 gap junction hemichannels became visible. In the presence of Ca^{2+}, the hemichannel surface structures moved radially to close the channel entrance (Figure 4). This closure was reversed with the removal of Ca^{2+}. In presence of aminosulfonate compounds, the gating of gap junction hemichannels is pH-dependent. Watching the pH-induced gating in the presence of the aminosulfonate compound HEPES showed the gap junction surface structures rotate like an "iris" shutter to close and open the channel entrance (*50*). In spite of the importance of intercellular channels in diseases, which other functional gating mechanisms may have evolved, what their advantages are, and how they are controlled remain to be elucidated.

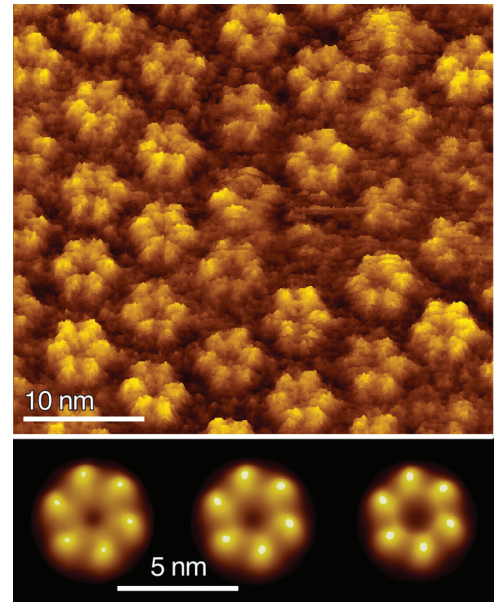

FIGURE 4: Watching communication channels at work. High-resolution AFM topograph showing the extracellular surface of Cx26 gap junction hemichannels. The gap junction membranes have been dissected with the AFM probe to expose their extracellular surface (*27*). The bottom row shows the conformational change of hemichannels in response to Ca^{2+}. The closed channels (left) switch, via an intermediate conformation (middle), to the open state (right) in the presence of 0.5 mM Ca^{2+}. Hemichannels in the bottom row represent correlation averages.

Recently high-speed atomic force microscopes have been developed that are able to record up to 200 topographs per second (*52–54*). Their impact on the study of biological objects is difficult to predict, but the first publications imaging the conformational cycle of the molecular chaperone complexes GroEL/ES (*52, 53*), DNA cleavage (*55*), and the motor protein myosin (*56*) in action provide exciting insights. Surely, this high-speed nanoscale imaging will power the understanding of dynamic molecular biological processes.

Multifunctional High-Resolution Imaging. To complement the topographical information, AFM probes can be modified to simultaneously detect additional surface properties. Various modifications of scanning probes have been introduced over the past two decades (*4*). In this section, we discuss examples that demonstrate the potential of these probes in characterizing biological membranes. The simplest application uses an untreated AFM probe to both image membranes and localize electrostatic potentials. The negatively charged Si_3N_4 probe contours the height profile of a biological membrane at a constant force. Electrostatic interactions between the scanning probe and the membrane contribute to the force. If repulsive, the electrostatic interactions push the probe farther away and increase the height profile at which the membrane is contoured (*24*). The electrostatic double-layer interactions depend on the electrolyte concentration and valency of the buffer ions (*23*). Consequently, height profiles recorded in the presence and absence (screened

in sufficient electrolyte) of electrostatic interactions, or under different electrostatic conditions, reveal electrostatic surface potentials that can readily be converted into charge densities (*24, 57*). The lateral resolution of this method approaches tens of nanometers and is sufficient for locating charge differences between or within membrane patches (*57, 58*).

Using an approach similar to the one described above, AFM was employed to detect and locate the electrostatic potential generated by OmpF porin (*59*). The transmembrane channel formed by OmpF porin from *E. coli* contains charged residues, which are thought to form a filter that selects positively against negatively charged ions. This selectivity vanishes with an increasing electrolyte concentration. To detect the electrostatic potential generated by the OmpF porin channel, the reconstituted membrane proteins were imaged at a lateral resolution of ≈0.5 nm and a vertical resolution of ≈0.1 nm at variable electrolyte concentrations. This revealed the presence of an electrostatic potential at low electrolyte concentrations.

While the examples given above used untreated AFM probes to detect electrostatic interactions, other approaches employ modified probes. With such modifying probes, it is possible to detect hydrophilic and hydrophobic interactions, ion conductance, and electrochemical interactions (*4, 5*). Most of these examples could reveal interactions and map these at lateral resolutions ranging from 10 to 200 nm. However, the Engel group recently developed electrically insulated probes that are conductive only at their tip (*60*). The probes, mounted onto a soft cantilever (≤0.1 N/m), are sufficiently sharp to realize a lateral resolution of ≈8 nm. Individual pores of these S-layers were clearly resolved, and the conductive probe could measure currents at an accuracy of <1 pA (*60*). Such inventions foster the hope that in the near future AFM-related techniques will allow the imaging of native ion channels at high resolution while simultaneously performing spectroscopic measurements to characterize their conductive properties and gating mechanisms.

Probing Unfolding and Folding Pathways of Membrane Proteins. Pushing an AFM probe onto a polypeptide forces them to attach to each other (*61*). In single-molecule force spectroscopy (SMFS), this unspecific attachment is used to probe the interactions of proteins, nucleic acids, and polysaccharides (*62, 63*). Once the molecule of interest is attached, the AFM probe is withdrawn to distort the bound structure while the cantilever deflection recorded. The resulting force−distance ($F-D$) curve reveals forces required to pull the molecule from the support. In the case in which the molecule is attached with one end to the AFM probe and the other end to the support, the $F-D$ spectrum depicts the stretching of the single molecule. If the molecule was initially folded, the $F-D$ spectrum measures the force required to unfold the molecule (*61*). Unfolded by this method, membrane proteins unfold in distinct steps (*64, 65*). These unfolding steps indicate unfolding intermediates and constitute an unfolding pathway. Interestingly, the same membrane protein can unfold by different pathways (*66*). The probability with which a pathway protein unfolds is sensitive to environmental conditions. For example, different temperatures favored certain bacteriorhodopsin unfolding pathways (*67*). Similarly, the oligomeric state of the membrane protein (*68*), the specific binding of divalent ions (*69*), and mutations (*70, 71*) influence which pathways prevail.

SMFS was used to study the refolding of individual transmembrane segments of the Na^+/H^+ antiporter NhaA from *E. coli* (*72*). After the terminal end of the antiporter was attached to the AFM probe, a mechanical pulling force was applied to sequentially unfold structural segments. After unfolding and extraction of the first 10 of 12 α-helices, the unfolded polypeptide was relaxed to allow refolding into the membrane. After the polypeptide was given time to refold, the AFM probe was again retracted to determine the extent of refolding. At sufficiently long refolding times, >5 s, the polypeptide folded back into the native structure. Interestingly, some structural segments folded faster than others. Thus, with the variation in the refolding time, the refolding kinetics of individual structural segments were examined (*72*). It became evident that the extent of refolding influenced the stability of the folded segments. This experimental approach was also applied to bacteriorhodopsin (*73*).

The simplicity of SMFS makes it suitable for characterization of the unfolding and refolding of membrane proteins under near-physiological conditions. There are several advantages over conventional unfolding experiments that use chemical or thermal denaturation. The most obvious advantages are that SMFS characterizes the unfolding of membrane proteins embedded in their functionally important lipid membrane whereas conventional experiments study the unfolding of detergent-solubilized proteins. For SMFS, membrane proteins can either be reconstituted in lipid bilayers (*68, 72, 74*) or characterized in their native membrane (*65, 68*). In contrast to conventional unfolding experiments in which the unfolded state of the proteins is defined by the loss of their native structure, in SMFS the unfolded state is the fully stretched conformation. Thus, in SMFS the folded and unfolded states are structurally defined. Therefore, SMFS can be used to unravel the unfolding pathways of single proteins, estimate the probability of unfolding along these pathways, and assign unfolding intermediates along pathways.

Probing Interactions between and within Membrane Proteins. Each peak of an $F-D$ curve recorded during the unfolding of a single-membrane protein detects interactions that stabilize structural segments of the protein. These structural segments can represent polypeptide loops, secondary structure elements, or fragments or combinations thereof (*66, 75*). While the position of the force peak denotes the location of the structure (Figure 5), the force measures the strength stabilizing the segment. The physical and chemical origins of interactions acting in and between membrane proteins are manifold (*29, 76*). To decipher the conservative and dissipative components of these interactions, membrane proteins were unfolded using an oscillating AFM probe (*77, 78*). SMFS can be applied to characterize the extent to which inter- and intramolecular interactions contribute to structural regions within membrane proteins. Thus, SMFS was applied to characterize the interactions of membrane proteins assembled into different oligomeric states (*68, 79*), attached to signaling polypeptides (*80*), being mutated (*70, 71*), and being exposed to different electrolytes (*69*), pH values (*81*), and temperatures (*67*).

Detecting and Locating Ligand and Inhibitor Binding to Membrane Proteins. While molecular interactions determine the folding and stability of proteins, they also determine their functional state (*29, 76*). The interactions in an inactive state

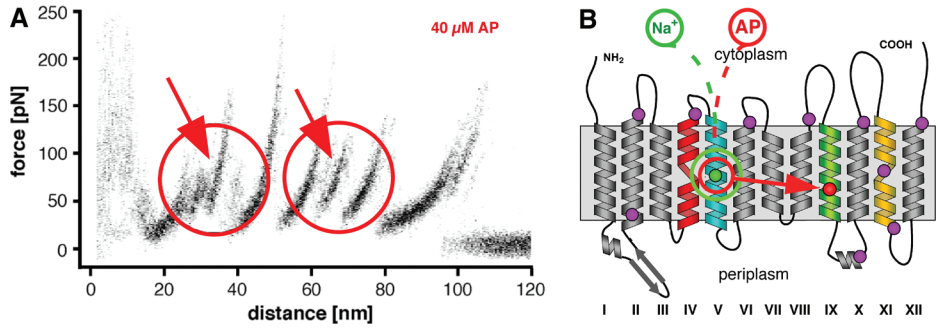

FIGURE 5: SMFS detects and locates functionally relevant interactions within membrane proteins. (A) Superimposition of $F-D$ spectra recorded upon unfolding the Na^+/H^+ antiporter NhaA from *E. coli* in the presence of the inhibitor 2-aminoperimidine (AP). Every force peak detected in the $F-D$ curves reflects interactions that have been established within NhaA. Fitting these force peaks with the wormlike chain model allows us to locate their interactions (B) on the secondary structure of NhaA. (B) Filled circles denote the locations of interactions detected by SMFS. Binding of the inhibitor significantly enhances two interactions (red circles in panel A). This inhibitor binding mimics the interactions established by ligand binding (green filled circle) and significantly (≈50%) enhances the interaction located at transmembrane α-helix IX (red filled circle) (*83*). In contrast, binding of the ligand (a single Na^+ ion, colored green) establishes an interaction only at the ligand-binding site (green filled circle) (*81*).

are different from those established in an activated state. Kedrov et al. performed SMFS to detect the interactions of the inactive and active states of the Na^+/H^+ antiporter NhaA (*81*). Surprisingly, these single-molecule experiments revealed a clear difference between the antiporter's functional states (Figure 5). Additional interactions are established upon the binding of ligand (a Na^+ ion) to its binding pocket. Similar results were obtained when the ligand binding-induced activation of another Na^+/H^+ antiporter was studied (*82*). In the next experiment, Kedrov et al. showed that SMFS also detects the binding of an inhibitor to the antiporter NhaA (*83*). The inhibitor competes with the ligand for the binding pocket and, upon binding, mimics the interaction of the ligand but, in addition to ligand binding, establishes an interaction at an α-helix that functionally deactivates NhaA. These results demonstrate that the AFM probe can be used to directly visualize ligand-gated conformational changes in single-membrane proteins (Figure 4) and to detect and locate the binding of a ligand or an inhibitor (Figure 5). The SMFS spectrum itself can serve as a fingerprint of the protein's functional state (*75*). In the future, SMFS may be applied as a screening method to detect and locate the binding of small molecules or drugs that direct the functional state of membrane proteins. Such approaches are particularly important since membrane proteins constitute the predominant targets for drug research and development.

Probing Specific Interactions of Cellular Membranes. Via functionalization of the AFM probe, specific interactions with biological membranes can be detected (Figure 1). These measurements can be performed with both membranes in living cells and membranes isolated and adsorbed onto a supporting surface. To conduct SMFS, an AFM probe is modified with a ligand and brought into contact with its receptor (*84*). After a preset contact time, the probe is retracted from the receptor and the cantilever deflection measured. The rupture of interactions between the ligand and receptor is detected by a force deflecting the cantilever (*84*). Measuring this force over several pulling velocities (force-loading rate) allows the energy landscape of the ligand−receptor interaction to be reconstructed (*85*) (see the following sections on energy landscapes for details). To retain sufficient mobility of the ligand and to separate the frequently occurring unspecific interactions between the probe and membrane, the ligand is attached to the probe via a flexible spacer that is several nanometers in length (*86*).

The group of Hinterdorfer used this approach to image membrane surfaces and map their functional groups (*86*). In this so-called molecular recognition imaging mode, membrane topography and information about locations at which ligands bind are gained. To map molecular recognition events, the atomic force microscope records $F-D$ curves at every topographic pixel. Currently, the time required (≈15 min) to record such adhesion maps, the force sensitivity and dynamic response of suitable AFM cantilevers, and the spatial resolution (10−100 nm) do not allow this method to follow the dynamic processes of cellular membranes (*86*). However, atomic force microscopes allowing faster probing together with cantilevers enabling a higher force resolution will extend the current limits of this approach.

Single Cells as Molecular Probes. Cell adhesion determines or at least contributes to most cellular processes from the mating of two haploid yeast cells to the biogenesis of complex organs. Cell adhesion is commonly defined as the binding of a cell to a substrate, which can be another cell, a surface, or a matrix. The process of cell adhesion is regulated by specific cell adhesion molecules (CAMs) that are located on the cell surface and involved in substrate binding. In single-cell force spectroscopy (SCFS) (*87, 88*), a single living cell is attached to an AFM cantilever and employed as a probe (Figure 6A). Like SMFS, in SCFS the cellular probe if brought into contact with a support or another cell for a set contact time and force. Thereafter, while the cell is separated from the support, an $F-D$ curve records the cellular interactions. The $F-D$ curve describing the separation of a cell from a substrate can be split into three phases (Figure 6B). In the initial phase (c.1), the cantilever retraction inverts the force acting on the cell from pushing to pulling. With an increase in pulling force, the forces acting on individual cell−substrate adhesion points increase. If many receptors act in concert, the applied force is sufficiently high to deform the cell cortex. The receptor binding strengths as well as their number and geometric placement determine the force at which the cell will start to detach. This detachment force (F_{detach}) represents the largest adhesion force of cell−substrate binding. After the cell starts detaching, individual force steps can be observed. These steps reflect

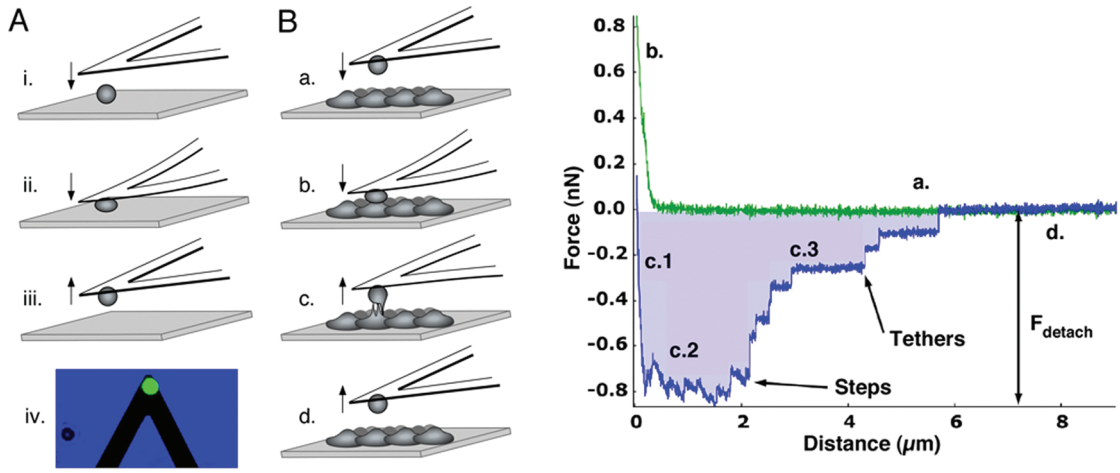

FIGURE 6: Using a single cell to probe cellular interactions at molecular resolution. (A) (i) The apex of a lectin-functionalized (often concavalin A) tip-less AFM cantilever is positioned above a cell. (ii) The cantilever is gently pushed (<1 nN) on the cell until the cell adheres. (iii) Separating the cantilever from the support detaches the cell from its substrate and allows the bound cell to establish firm adhesion to the cantilever. (iv) Fluorescence microscopy image of a cell (green) bound to a tip-less cantilever. (B) (a) The cantilever functionalized with the living cell is positioned over other cells. (b) The cell is gently pushed (<1 nN) onto the cells of interest for a preset contact time. The green $F-D$ curve reports this approach process until a threshold force of ≈0.85 nN is reached. (c) Then the cantilever is retracted to separate probing and probed cells. The cantilever deflection measures the interaction between both cells over the separation in an $F-D$ curve (blue curve). This curve provides a signature of the cell adhesion and can be separated into several processes (c.1−3). The steadily increasing force occurring at the beginning of the cell−cell separation (c.1) describes the increasing strain on the cells leading to the rupture of bonds formed between the cells (c.2). The maximum force measured is termed the detachment force (F_{detach}). During separation, membrane tethers (c.3) can be pulled out of the cell. Tethers are characterized by long plateaus at constant force. The area shaded blue represents the work required to detach the cells from each other.

the rupture of individual receptor−ligand interactions. During this second phase (c.2 in Figure 6B), the receptors either detach from the substrate or are pulled away from the cell cortex at the tip of membrane tethers. While parts of the cortex are in contact, either of these may occur. The third phase of detachment (c.3) occurs when the cell body is no longer in contact with the substrate and, thus, attachment is exclusively by tethers.

Like SMFS, SCFS can detect the interaction of single receptor−ligand pairs. However, SMFS measures these interactions using purified transmembrane receptors that have been removed from their cellular environment and have been very often truncated and consist of only their extracellular domains. Thus, one cannot be sure of their functional state. This is of particular concern with receptors (such as integrins) that have several substrate binding affinity states and can be regulated via interactions with cytoplasmic factors from the cell. In contrast to SMFS, SCFS examines receptor−ligand interactions in their functional cellular environment (*88*). Using a living cell as a probe ensures that the receptors are native and, moreover, the mechanisms by which they are regulated can be examined. Indeed, comparing interaction strengths of isolated receptors and of receptors embedded in their native cellular environment sometimes reveals different values (*88*). However, applying single-molecule evaluation methods in experiments using cell-bound receptors has special problems. First and foremost is the heterogeneity of possible cell surface interactions. Special care has to be taken to ensure that the single-molecule interactions recorded are predominantly, if not exclusively, between the receptor and ligand of interest. To this end, recombinant substrates are often used and cells may be genetically modified to limit the number of receptors expressed. Control experiments demonstrating the specificity of the observed interactions must be performed. Thus, excellent molecular cell biology

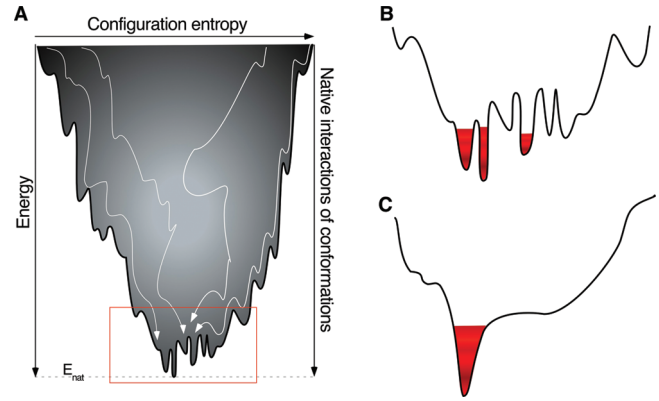

FIGURE 7: Schematic illustration of an energy landscape that could describe the folding of a polypeptide. (A) The folding of a polypeptide into a native protein structure is funneled by the formation of interactions and structural conformations. The width and depth of the funnel describe the entropy and energy of the folding reaction, respectively. Discrete folding pathways (white lines) on which the folding polypeptide moves to increase its number of native interactions may coexist. The native folded protein at the bottom of the energy landscape is stabilized at the lowest energy, E_{nat}. A rugged bottom of the energy landscape (red rectangle zoomed out in panel B) indicates that the energetic contributions cannot be simultaneously minimized in a single conformation. Such a "frustrated" protein can adopt alternate conformational substates each having a certain probability (indicated by red colors). (C) A smooth landscape indicates that the different interactions contributing to the conformation at the bottom are "minimally frustrated".

is required to use SCFS and to answer pertinent questions about cell−cell and cell−substrate interactions.

Probing Energy Landscapes. The fundamental concept of energy landscapes (Figure 7) is important to the understanding of how biological reactions, such as folding, functional activation, ligand binding, and adhesion, take place (*89*). We are in an exciting situation: SMFS not only can detect the

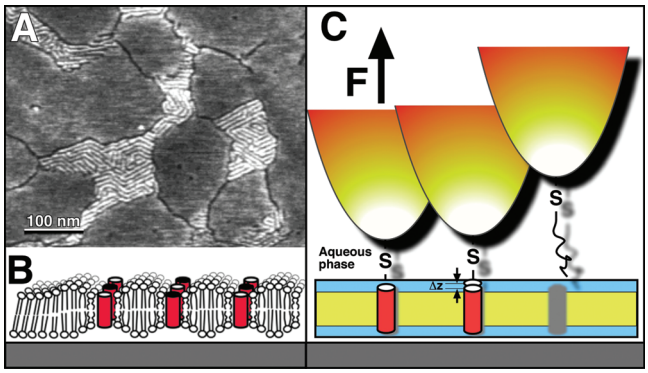

FIGURE 8: Imaging and manipulating transmembrane SH-WLAP23 polypeptides within DPPC bilayers. (A) An AFM topograph of striated domains in 2 mol % WLAP23-containing bilayers. Striated domains (ripples), cracks, and flat bilayer are shown (*12*). (B) Schematic of organization of striated domains. (C) Illustration of the SMFS experiment in which single-WLAP23 polypeptides were pulled out of the lipid bilayer. The WLAP23 polypeptide is attached via a covalent bond to the chemically functionalized AFM probe. At sufficiently high pulling forces, the WLAP23 polypeptide unfolds and is removed from the bilayer. DFS pulling of individual WLAP23 domains at different loading rates suggests that stretching of the folded polypeptide with a Δz of ≈0.75 nm is sufficient to induce its unfolding and removal (*92*).

interactions stabilizing functional states of a biomolecular system but also can probe its energy landscape. To do so, SMFS is used to probe the strength of molecular interactions at different loading rates (force applied over time) in a mode called dynamic single-molecule force spectroscopy (DFS). This reveals details of the energy landscape such as the distance from the folded to transition state, the height of the energy barrier stabilizing the folded state, and the lifetime of the folded state (*85*). In the past, DFS provided insight into how, e.g., ligand or inhibitor binding modulates interactions and consequently alters the energy landscape of a receptor (*90*). Other studies determined the energy barriers that anchor transmembrane α-helices in lipid bilayers. Moreover, DFS monitored how structural (e.g., mutations, assembly) and environmental (e.g., pH, electrolyte) changes affect the complex interaction networks and the energy landscape of a membrane protein. The following sections will provide an overview of DFS as it is applied in characterizing interactions and energy landscapes of biological membranes and their components.

Probing the Interactions and Energy Landscape of Short Polypeptides and Membranes. The interactions of hydrophobic and hydrophilic polypeptides with membrane bilayers are fundamentally significant for the folding, assembly, and function of membrane proteins. Proteins with single-transmembrane α-helices are involved in signal transduction, restructuring of lipid mono- and bilayers, membrane fusion, compartmentalization, and many other processes within biological membranes. As with SMFS performed on membrane proteins composed of multiple transmembrane α-helices or β-sheets, an AFM probe functionalized with a short polypeptide is a versatile nanotool for probing their behavior (compare Figure 1). Synthetic polypeptides can be designed to systematically characterize the contribution of single amino acids to the interactions of a given polypeptide segment with a membrane bilayer (*29, 91*). In an attempt to characterize such interaction mechanisms, the de Kruijff group measured the integration forces of synthetic WALP23 polypeptides with DPPC and DOPC bilayers (*92*). By extracting individual WALP23 polypeptides from the bilayer (Figure 8), they determined rupture forces which varied with loading rates from ≈55 pN at 0.1 nN/s to 95 pN at 45 nN/s. A single energy barrier with a length of 0.75 nm separated the membrane inserted from the unfolded state of the polypeptide. Thus, the transmembrane α-helix formed by the WALP23 polypeptide must be only mechanically stretched by this distance to initiate unfolding and extraction from the membrane. A similar approach using DFS and steered molecular dynamics (SMD) simulations was used to characterize the interactions of CWALP[19]23 polypeptides with DPPC and DSPC bilayers (*93*). It showed that the unfolding transition state was separated from the state by only ≈0.3 nm (*93*).

Probing the Interactions and Energy Landscape of Membrane Proteins. DFS can be used to detect the dynamic response of interactions within membrane proteins (*94*). DFS experiments with bacteriorhodopsin revealed that the unfolding of individual transmembrane α-helices was initiated upon the stretching of their folded states by ≈0.5 nm (*95*). This indicates that extending transmembrane α-helices by less than 10% of their length may trigger their unfolding. Transmembrane α-helices of bacteriorhodopsin unfold individually or as pairs (*67*). The transition rates characterizing these unfolding events are $\approx 10^{-2}$ s^{-1} for single α-helices and $\approx 10^{-4}$ s^{-1} for α-helical pairs (*95*). Thus, the typical stability of a single α-helix is ≈100 s and that of a pair of α-helices $\approx 10^4$ s at room temperature. These values compare well with those of water-soluble proteins (*95*) and highlight the role of α-helices as folding intermediates of membrane proteins (*96*).

The topography of the folding energy landscape determines the dynamics of the reaction kinetics of folding. Smooth energy landscapes are linked to fast folding kinetics, while rough surfaces predict the transient trapping in local energy minima (*89*). Using DFS, Janovjak et al. (*97*) measured the energy landscape roughness for the unfolding of individual transmembrane α-helices within bacteriorhodopsin (Figure 9). The calculated surface ruggedness of $\approx 5k_BT$ is in the same range as that measured for short polypeptides, DNA strands, two interacting proteins, and small water-soluble proteins.

In other examples, DFS was employed to detect variations in interactions induced within bacteriorhodopsin by the insertion of single point (*70*) or triple (*71*) mutations. Depending on the structural position into which the mutations were inserted, they could change interactions stabilizing the structural segment hosting the mutations and/or of interactions stabilizing structural segments distant from the mutations. If the mutation changed the energy barrier of a structural segment, the energy difference between the folded and unfolded state decreased with the distance between the folded and transition states. This was the first time that the so-called Hammond postulate could be demonstrated for membrane proteins (*70*). However, confirmations of this correlation for other membrane proteins are needed. The possibility of precisely determining how and where mutations change the interactions and the energy landscape of membrane proteins may explain which mutations and factors lead to membrane protein destabilization and malfunction (*98*).

Observing Mechanisms by Which an Inhibitor Deactivates a Membrane Protein. Membrane proteins can selectively bind solutes from the cytoplasm or extracellular space. This binding may modulate inter- and intramolecular interactions,

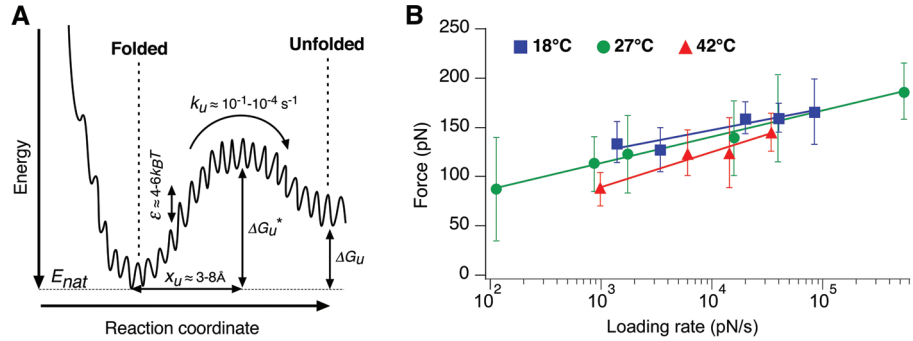

FIGURE 9: Determining the energy landscape roughness of individual transmembrane α-helices of a membrane protein. (A) A simple two-state barrier describes the unfolding of an α-helix. Parameters shown describe the roughness (ε), of the energy landscape, the distance between the folded and transition state (x_u), the transition rate in the absence of an applied force (k_u), and the unfolding free energy (ΔG_u). All parameters represent ranges measured for all α-helices. (B) Unfolding forces of transmembrane helices depend on force loading rates. The forces were measured for the pairwise unfolding of transmembrane α-helices B and C of bacteriorhodopsin. Plotting the most probable force against the logarithm of the loading rate yields a single linear regime, which suggests a single potential barrier such as that shown in panel A. The experimental data show the unfolding forces measured at different temperatures. Since the unfolding process is thermally driven, the energy landscape is temperature-dependent. Fitting the experimental data reveals this temperature dependency. Accordingly, the x_u and k_u values for α-helices B and C are 7.67 ± 0.03 Å and 2.7 × 10^{-5} s^{-1} at 18 °C, 6.52 ± 1.65 Å and 7.0 × 10^{-4} s^{-1} at 27 °C, and 4.11 ± 0.40 Å and 8.1 × 10^{-2} s^{-1} at 42 °C, respectively (*97*). The roughness of the energy surface of α-helices B and C [ε = 22.3 pN/nm (≈5k_BT)] could be reconstructed from these temperature-dependent data.

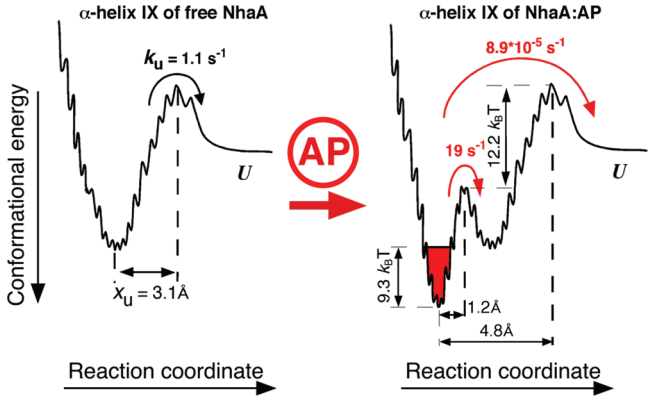

FIGURE 10: Following the dynamic energy landscape upon binding of an inhibitor to an antiporter. The inhibitor 2-aminoperimidine (AP) binds to the ligand-binding pocket of the Na^+/H^+ antiporter NhaA. SMFS detects that this binding establishes additional interactions at the ligand-binding site and at transmembrane α-helix IX (Figure 5). The dynamic behavior of these interactions was characterized via DFS. In the case of α-helix IX, we found that the stabilizing energy barrier changed dynamically upon AP binding. The energy valley showed a lower energy in the inhibited state and a much narrower width. Both effects stabilize and at the same time restrict the conformational flexibility of helix IX (*100*).

the energy landscape, and functional state (*89*). Understanding the mechanistic nature of binding events controlling a target is a central topic in modern drug discovery. SMFS experiments on the Na^+/H^+ antiporter NhaA (*81*) detected and differentiated between interactions induced by the binding of a ligand and of an inhibitor (Figure 5). The inhibitor 2-aminoperimidine (AP) established interactions similar to those of the ligand within the ligand-binding pocket of the transporter but also significantly increased the strength of the interaction located at transmembrane α-helix IX (*83*). In contrast to all other α-helices of NhaA, α-helix IX exhibits an enhanced intrinsic flexibility that is believed to be functionally relevant (*99*). Thus, one may speculate that the inhibitor specifically enhances interactions at α-helix IX to alter the helix's structural flexibility (*83*). To test this hypothesis, DFS was applied in comparing the energy barriers stabilizing the α-helices of NhaA being set in the activated and inhibited state (*100*). The force versus loading rate plot of the free antiporter indicated that each α-helix is stabilized by a single energy barrier that separates the folded and transition states by 0.3−0.6 nm (*100*). In the AP-inhibited state, α-helix IX exhibited two energy barriers while all other α-helices remained unperturbed (Figure 10). The inner barrier stabilizing the folded state was found to exhibit a lower conformational energy and an approximately 3-fold narrower distance (≈0.1 nm) to the transition state. A reduced width of the energy valley stabilizing a structure further restricts the number of possible conformational states (Figure 7). Thus, Kedrov et al. (*100*) concluded that this new narrow energy barrier, formed by inhibitor binding, restricts the conformational flexibility of α-helix IX. This is the first example in which DFS was applied to show how the binding of a molecule to a membrane protein switches its functional state. In the future, SMFS-related approaches might be used to optimize drug binding and functional modulation of a target.

Concluding Remarks. AFM is a versatile nanotool for imaging biological membranes at subnanometer resolution and for specifically probing a wide range of properties. Examples discussed here provide a brief overview of the contribution AFM makes to membrane biology. Although a much broader spectrum of AFM-related methods has been developed (*4*), they have not yet found application in membrane biology. It is expected that these scanning probe techniques will in the next decades further extend the laboratory on a tip approach to characterizing native biological membranes in their native environment from the nanoscopic to the microscopic scale. Existing and developing AFM-related approaches will contribute multifunctional tools that reveal unique insights into pertinent questions in membrane biology.

ACKNOWLEDGMENT

I thank my colleagues Ch. Bippes, J. Helenius, S. Mari, T. Sapra, and S. Wegmann for stimulating discussions.

REFERENCES

1. Engelman, D. M. (2005) Membranes are more mosaic than fluid. *Nature 438*, 578–580.
2. Hell, S. W. (2007) Far-field optical nanoscopy. *Science 316*, 1153–1158.
3. Robinson, C. V., Sali, A., and Baumeister, W. (2007) The molecular sociology of the cell. *Nature 450*, 973–982.
4. Gerber, C., and Lang, H. P. (2007) How the doors to the nanoworld were opened. *Nat. Nanotechnol. 1*, 3–5.
5. Muller, D. J., and Dufrene, Y. (2008) Atomic force microscopy as a multifunctional molecular toolbox in nanobiotechnology. *Nat. Nanotechnol. 3*, 261–269.
6. Grandbois, M., Clausen-Schaumann, H., and Gaub, H. (1998) Atomic force microscope imaging of phospholipid bilayer degradation by phospholipase A2. *Biophys. J. 74*, 2398–2404.
7. Nielsen, L. K., Risbo, J., Callisen, T. H., and Bjornholm, T. (1999) Lag-burst kinetics in phospholipase A(2) hydrolysis of DPPC bilayers visualized by atomic force microscopy. *Biochim. Biophys. Acta 1420*, 266–271.
8. El Kirat, K., Dupres, V., and Dufrene, Y. F. (2008) Blistering of supported lipid membranes induced by phospholipase D, as observed by real-time atomic force microscopy. *Biochim. Biophys. Acta 1778*, 276–282.
9. Rigby-Singleton, S. M., Davies, M. C., Harris, H., O'Shea, P., and Allen, S. (2006) Visualizing the solubilization of supported lipid bilayers by an amphiphilic peptide. *Langmuir 22*, 6273–6279.
10. Pedersen, T. B., Kaasgaard, T., Jensen, M. O., Frokjaer, S., Mouritsen, O. G., and Jorgensen, K. (2005) Phase behavior and nanoscale structure of phospholipid membranes incorporated with acylated C14-peptides. *Biophys. J. 89*, 2494–2503.
11. Alattia, J. R., Shaw, J. E., Yip, C. M., and Prive, G. G. (2007) Molecular imaging of membrane interfaces reveals mode of β-glucosidase activation by saposin C. *Proc. Natl. Acad. Sci. U.S.A. 104*, 17394–17399.
12. Rinia, H. A., Boots, J. W., Rijkers, D. T., Kik, R. A., Snel, M. M., Demel, R. A., Killian, J. A., van der Eerden, J. P., and de Kruijff, B. (2002) Domain formation in phosphatidylcholine bilayers containing transmembrane peptides: Specific effects of flanking residues. *Biochemistry 41*, 2814–2824.
13. Chiantia, S., Kahya, N., and Schwille, P. (2007) Raft domain reorganization driven by short- and long-chain ceramide: A combined AFM and FCS study. *Langmuir 23*, 7659–7665.
14. Giocondi, M. C., Besson, F., Dosset, P., Milhiet, P. E., and Le Grimellec, C. (2007) Remodeling of ordered membrane domains by GPI-anchored intestinal alkaline phosphatase. *Langmuir 23*, 9358–9364.
15. Czajkowsky, D. M., and Shao, Z. (2002) Supported lipid bilayers as effective substrates for atomic force microscopy. *Methods Cell Biol. 68*, 231–241.
16. Muller, D. J., Engel, A. (2008) Strategies to prepare and characterize native membrane proteins and protein membranes by AFM. *Curr. Opin. Colloid Interface Sci*. (in press)
17. Muller, D. J., and Engel, A. (2007) Atomic force microscopy and spectroscopy of native membrane proteins. *Nat. Protoc. 2*, 2191–2197.
18. Muller, D. J., Schoenenberger, C. A., Büldt, G., and Engel, A. (1996) Immuno-atomic force microscopy of purple membrane. *Biophys. J. 70*, 1796–1802.
19. Scheuring, S., Ringler, P., Borgina, M., Stahlberg, H., Muller, D. J., Agre, P., and Engel, A. (1999) High resolution topographs of the *Escherichia coli* waterchannel aquaporin Z. *EMBO J. 18*, 4981–4987.
20. Fotiadis, D., Suda, K., Tittmann, P., Jeno, P., Philippsen, A., Muller, D. J., Gross, H., and Engel, A. (2002) Identification and structure of a putative Ca^{2+}-binding domain at the C terminus of AQP1. *J. Mol. Biol. 318*, 1381–1394.
21. Heymann, J. B., Pfeiffer, M., Hildebrandt, V., Fotiadis, D., de Groot, B., Kabak, R., Engel, A., Oesterhelt, D., and Muller, D. J. (2000) Conformations of the rhodopsin third cytoplasmic loop grafted onto bacteriorhodopsin. *Structure 8*, 643–644.
22. Engel, A., and Muller, D. J. (2000) Observing single biomolecules at work with the atomic force microscope. *Nat. Struct. Biol. 7*, 715–718.
23. Butt, H.-J., Jaschke, M., and Ducker, W. (1995) Measuring surface forces in aqueous solution with the atomic force microscope. *Bioelectrochem. Bioenerg. 38*, 191–201.
24. Muller, D. J., and Engel, A. (1997) The height of biomolecules measured with the atomic force microscope depends on electrostatic interactions. *Biophys. J. 73*, 1633–1644.
25. Muller, D. J., Sapra, K. T., Scheuring, S., Kedrov, A., Frederix, P. L., Fotiadis, D., and Engel, A. (2006) Single-molecule studies of membrane proteins. *Curr. Opin. Struct. Biol. 16*, 489–495.
26. Scheuring, S., Muller, D. J., Stahlberg, H., Engel, H. A., and Engel, A. (2002) Sampling the conformational space of membrane protein surfaces with the AFM. *Eur. Biophys. J. 31*, 172–178.
27. Muller, D. J., Hand, G. M., Engel, A., and Sosinsky, G. (2002) Conformational changes in surface structures of isolated Connexin26 gap junctions. *EMBO J. 21*, 3598–3607.
28. Muller, D. J., Sass, H.-J., Muller, S., Büldt, G., and Engel, A. (1999) Surface structures of native bacteriorhodopsin depend on the molecular packing arrangement in the membrane. *J. Mol. Biol. 285*, 1903–1909.
29. White, S. H., and Wimley, W. C. (1999) Membrane protein folding and stability: Physical principles. *Annu. Rev. Biophys. Biomol. Struct. 28*, 319–365.
30. Sapra, K. T., Park, P. S., Palczewski, K., and Muller, D. J. (2008) Mechanical properties of bovine rhodopsin and bacteriorhodopsin: Possible roles in folding and function. *Langmuir 24*, 1330–1337.
31. Hoh, J. H., Lal, R., John, S. A., Revel, J.-P., and Arnsdorf, M. F. (1991) Atomic force microscopy and dissection of gap junctions. *Science 253*, 1405–1408.
32. Fotiadis, D., Hasler, L., Muller, D. J., Stahlberg, H., Kistler, J., and Engel, A. (2000) Surface tongue-and-groove contours on lens MIP facilitate cell-to-cell adherence. *J. Mol. Biol. 300*, 779–789.
33. Fotiadis, D., Muller, D. J., Tsiotis, G., Hasler, L., Tittmann, P., Mini, T., Jenö, P., Gross, H., and Engel, A. (1998) Surface analysis of the photosystem I complex by electron and atomic force microscopy. *J. Mol. Biol. 283*, 83–94.
34. Scheuring, S., Seguin, J., Marco, S., Levy, D., Robert, B., and Rigaud, J. L. (2003) Nanodissection and high-resolution imaging of the *Rhodopseudomonas viridis* photosynthetic core complex in native membranes by AFM. *Proc. Natl. Acad. Sci. U.S.A. 100*, 1690–1693.
35. Czajkowsky, D. M., Sheng, S., and Shao, Z. (1998) Staphylococcal α-hemolysin can form hexamers in phospholipid bilayers. *J. Mol. Biol. 276*, 325–330.
36. Mou, J. X., Yang, J., and Shao, Z. F. (1995) Atomic force microscopy of cholera toxin B-oligomers bound to bilayers of biologically relevant lipids. *J. Mol. Biol. 248*, 507–512.
37. Seelert, H., Poetsch, A., Dencher, N. A., Engel, A., Stahlberg, H., and Muller, D. J. (2000) Proton powered turbine of a plant motor. *Nature 405*, 418–419.
38. Stahlberg, H., Muller, D. J., Suda, K., Fotiadis, D., Engel, A., Matthey, U., Meier, T., and Dimroth, P. (2001) Bacterial ATP synthase has an undecameric rotor. *EMBO Rep. 21*, 1–5.
39. Pogoryelov, D., Yu, J., Meier, T., Vonck, J., Dimroth, P., and Muller, D. J. (2005) The c15 ring of the *Spirulina platensis* F-ATP synthase: F1/F0 symmetry mismatch is not obligatory. *EMBO Rep. 6*, 1040–1044.
40. Fotiadis, D., Liang, Y., Filipek, S., Saperstein, D. A., Engel, A., and Palczewski, K. (2003) Atomic-force microscopy: Rhodopsin dimers in native disc membranes. *Nature 421*, 127–128.
41. Fotiadis, D., Jastrzebska, B., Philippsen, A., Muller, D. J., Palczewski, K., and Engel, A. (2006) Structure of the rhodopsin dimer: A working model for G-protein-coupled receptors. *Curr. Opin. Struct. Biol. 16*, 252–259.
42. Cisneros, D. A., Oesterhelt, D., and Muller, D. J. (2005) Probing origins of molecular interactions stabilizing the membrane proteins halorhodopsin and bacteriorhodopsin. *Structure 13*, 235–242.
43. Klyszejko, A. L., Shastri, S., Mari, S. A., Grubmuller, H., Muller, D. J., and Glaubitz, C. (2008) Folding and assembly of proteorhodopsin. *J. Mol. Biol. 376*, 35–41.
44. Scheuring, S., and Sturgis, J. N. (2005) Chromatic adaptation of photosynthetic membranes. *Science 309*, 484–487.
45. Fotiadis, D., Qian, P., Philippsen, A., Bullough, P. A., Engel, A., and Hunter, C. N. (2004) Structural analysis of the reaction center light-harvesting complex I photosynthetic core complex of *Rhodospirillum rubrum* using atomic force microscopy. *J. Biol. Chem. 279*, 2063–2068.
46. Hoogenboom, B. W., Suda, K., Engel, A., and Fotiadis, D. (2007) The supramolecular assemblies of voltage-dependent anion channels in the native membrane. *J. Mol. Biol. 370*, 246–255.
47. Muller, D. J., Baumeister, W., and Engel, A. (1996) Conformational change of the hexagonally packed intermediate layer of

Deinococcus radiodurans imaged by atomic force microscopy. *J. Bacteriol. 178*, 3025–3030.
48. Muller, D. J., and Engel, A. (1999) Voltage and pH-induced channel closure of porin OmpF visualized by atomic force microscopy. *J. Mol. Biol. 285*, 1347–1351.
49. Jaroslawski, S., Zadek, B., Ashcroft, F., Venien-Bryan, C., and Scheuring, S. (2007) Direct visualization of KirBac3.1 potassium channel gating by atomic force microscopy. *J. Mol. Biol. 374*, 500–505.
50. Yu, J., Bippes, C. A., Hand, G. M., Muller, D. J., and Sosinsky, G. E. (2007) Aminosulfonate modulated pH-induced conformational changes in connexin26 hemichannels. *J. Biol. Chem. 282*, 8895–8904.
51. Andersen, C., Schiffler, B., Charbit, A., and Benz, R. (2002) pH-induced collapse of the extracellular loops closes *Escherichia coli* maltoporin and allows the study of asymmetric sugar binding. *J. Biol. Chem. 277*, 41318–41325.
52. Viani, M. B., Pietrasanta, L. I., Thompson, J. B., Chand, A., Gebeshuber, I. C., Kindt, J. H., Richter, M., Hansma, H. G., and Hansma, P. K. (2000) Probing protein-protein interactions in real time. *Nat. Struct. Biol. 7*, 644–647.
53. Yokokawa, M., Wada, C., Ando, T., Sakai, N., Yagi, A., Yoshimura, S. H., and Takeyasu, K. (2006) Fast-scanning atomic force microscopy reveals the ATP/ADP-dependent conformational changes of GroEL. *EMBO J. 25*, 4567–4576.
54. Humphris, A. D., Miles, M., and Hobbs, J. K. (2005) A mechanical microscope: High-speed atomic force microscopy. *Appl. Phys. Lett. 86*.
55. Yokokawa, M., Yoshimura, S. H., Naito, Y., Ando, T., Yagi, A., Sakai, N., and Takeyasu, K. (2006) Fast-scanning atomic force microscopy reveals the molecular mechanism of DNA cleavage by ApaI endonuclease. *IEE Proc.: Nanobiotechnol. 153*, 60–66.
56. Kodera, N., Kinoshita, T., Ito, T., and Ando, T. (2003) High-resolution imaging of myosin motor in action by a high-speed atomic force microscope. *Adv. Exp. Med. Biol. 538*, 119–127.
57. Yang, Y., Mayer, K. M., and Hafner, J. H. (2007) Quantitative membrane electrostatics with the atomic force microscope. *Biophys. J. 92*, 1966–1974.
58. Heinz, W. F., and Hoh, J. H. (1999) Relative surface charge density mapping with the atomic force microscope. *Biophys. J. 76*, 528–538.
59. Philippsen, A., Im, W., Engel, A., Schirmer, T., Roux, B., and Muller, D. J. (2002) Imaging the electrostatic potential of transmembrane channels: Atomic probe microscopy on OmpF porin. *Biophys. J. 82*, 1667–1676.
60. Frederix, P. L. T. M., Gullo, M. R., Akiyama, T., Tonin, A., de Rooij, N. F., Staufer, U., and Engel, A. (2005) Assessment of insulated conductive cantilevers for biology and electrochemistry. *Nanotechnology 16*, 997–1005.
61. Rief, M., Gautel, M., Oesterhelt, F., Fernandez, J. M., and Gaub, H. E. (1997) Reversible unfolding of individual titin immunoglobulin domains by AFM. *Science 276*, 1109–1112.
62. Rief, M., Oesterhelt, F., Heymann, B., and Gaub, H. E. (1997) Single molecule force spectroscopy on polysaccharides by AFM. *Science 275*, 1295–1298.
63. Rief, M., Clausen-Schaumann, H., and Gaub, H. E. (1999) Sequence-dependent mechanics of single DNA molecules. *Nat. Struct. Biol. 6*, 346–349.
64. Muller, D. J., Baumeister, W., and Engel, A. (1999) Controlled unzipping of a bacterial surface layer with atomic force microscopy. *Proc. Natl. Acad. Sci. U.S.A. 96*, 13170–13174.
65. Oesterhelt, F., Oesterhelt, D., Pfeiffer, M., Engel, A., Gaub, H. E., and Muller, D. J. (2000) Unfolding pathways of individual bacteriorhodopsins. *Science 288*, 143–146.
66. Muller, D. J., Kessler, M., Oesterhelt, F., Moeller, C., Oesterhelt, D., and Gaub, H. (2002) Stability of bacteriorhodopsin α-helices and loops analyzed by single-molecule force spectroscopy. *Biophys. J. 83*, 3578–3588.
67. Janovjak, H., Kessler, M., Gaub, H., Oesterhelt, D., and Muller, D. J. (2003) Unfolding pathways of native bacteriorhodopsin depend on temperature. *EMBO J. 22*, 5220–5229.
68. Sapra, K. T., Besir, H., Oesterhelt, D., and Muller, D. J. (2006) Characterizing molecular interactions in different bacteriorhodopsin assemblies by single-molecule force spectroscopy. *J. Mol. Biol. 355*, 640–650.
69. Park, P. S., Sapra, K. T., Kolinski, M., Filipek, S., Palczewski, K., and Muller, D. J. (2007) Stabilizing effect of Zn^{2+} in native bovine rhodopsin. *J. Biol. Chem. 282*, 11377–11385.
70. Sapra, K. T., Balasubramanian, G. P., Labudde, D., Bowie, J. U., and Muller, D. J. (2008) Point mutations in membrane proteins reshape energy landscape and populate different unfolding pathways. *J. Mol. Biol. 376*, 1076–1090.
71. Sapra, K. T., Doehner, J., Renugopalakrishnan, V., Padrós, E., and Muller, D. J. (2008) Role of extracellular glutamic acids in the stability and energy landscape of bacteriorhodopsin *Biophys. J.* (in press)
72. Kedrov, A., Janovjak, H., Ziegler, C., Kuhlbrandt, W., and Muller, D. J. (2006) Observing folding pathways and kinetics of a single sodium-proton antiporter from *Escherichia coli*. *J. Mol. Biol. 355*, 2–8.
73. Kessler, M., Gottschalk, K. E., Janovjak, H., Muller, D. J., and Gaub, H. E. (2006) Bacteriorhodopsin folds into the membrane against an external force. *J. Mol. Biol. 357*, 644–654.
74. Möller, C., Fotiadis, D., Suda, K., Engel, A., Kessler, M., and Muller, D. J. (2003) Determining molecular forces that stabilize human aquaporin-1. *J. Struct. Biol. 142*, 369–378.
75. Kedrov, A., Janovjak, H., Sapra, K. T., and Muller, D. J. (2007) Deciphering molecular interactions of native membrane proteins by single-molecule force spectroscopy. *Annu. Rev. Biophys. Biomol. Struct. 36*, 233–260.
76. Haltia, T., and Freire, E. (1995) Forces and factors that contribute to the structural stability of membrane proteins. *Biochim. Biophys. Acta 1228*, 1–27.
77. Janovjak, H., Muller, D. J., and Humphris, A. D. L. (2005) Molecular force modulation spectroscopy revealing the dynamic response of single bacteriorhodopsins. *Biophys. J. 88*, 1423–1431.
78. Bippes, C. A., Humphris, A. D., Stark, M., Muller, D. J., and Janovjak, H. (2006) Direct measurement of single-molecule viscoelasticity in atomic force microscope force-extension experiments. *Eur. Biophys. J. 35*, 287–292.
79. Janovjak, H., Sapra, K. T., and Muller, D. J. (2005) Complex stability of single proteins explored by forced unfolding experiments. *Biophys. J. 88*, L37–L39.
80. Cisneros, D. A., Oberbarnscheidt, L., Pannier, A., Klare, J. P., Helenius, J., Engelhard, M., Oesterhelt, F., and Muller, D. J. (2008) Transducer binding establishes localized interactions to tune sensory rhodopsin II. *Structure* . (in press).
81. Kedrov, A., Krieg, M., Ziegler, C., Kuhlbrandt, W., and Muller, D. J. (2005) Locating ligand binding and activation of a single antiporter. *EMBO Rep. 6*, 668–674.
82. Kedrov, A., Wegmann, S., Smits, S. H., Goswami, P., Baumann, H., and Muller, D. J. (2007) Detecting molecular interactions that stabilize, activate and guide ligand-binding of the sodium/proton antiporter MjNhaP1 from *Methanococcus jannaschii*. *J. Struct. Biol. 159*, 290–301.
83. Kedrov, A., Ziegler, C., and Muller, D. J. (2006) Differentiating ligand and inhibitor interactions of a single antiporter. *J. Mol. Biol. 362*, 925–932.
84. Moy, V. T., Florin, E.-L., and Gaub, H. E. (1994) Intermolecular forces and energies between ligands and receptors. *Science 266*, 257–259.
85. Evans, E. (1998) Energy landscapes of biomolecular adhesion and receptor anchoring at interfaces explored with dynamic force spectroscopy. *Faraday Discuss. 111*, 1–16.
86. Hinterdorfer, P., and Dufrene, Y. F. (2006) Detection and localization of single molecular recognition events using atomic force microscopy. *Nat. Methods 3*, 347–355.
87. Benoit, M., Gabriel, D., Gerisch, G., and Gaub, H. E. (2000) Discrete interactions in cell adhesion measured by single-molecule force spectroscopy. *Nat. Cell Biol. 2*, 313–317.
88. Helenius, J., Heisenberg, C. P., Gaub, H. E., and Muller, D. J. (2008) Single-cell force spectroscopy. *J. Cell Sci. 121*, 1785–1791.
89. Wolynes, P. G., Onuchic, J. N., and Thirumalai, D. (1995) Navigating the folding routes. *Science 267*, 1619–1620.
90. Evans, E. A., and Calderwood, D. A. (2007) Forces and bond dynamics in cell adhesion. *Science 316*, 1148–1153.
91. White, S. H., and von Heijne, G. (2005) Transmembrane helices before, during, and after insertion. *Curr. Opin. Struct. Biol. 15*, 378–386.
92. Ganchev, D. N., Rijkers, D. T., Snel, M. M., Killian, J. A., and de Kruijff, B. (2004) Strength of integration of transmembrane α-helical peptides in lipid bilayers as determined by atomic force spectroscopy. *Biochemistry 43*, 14987–14993.
93. Contera, S. A., Lemaitre, V., de Planque, M. R., Watts, A., and Ryan, J. F. (2005) Unfolding and extraction of a transmembrane

α-helical peptide: Dynamic force spectroscopy and molecular dynamics simulations. *Biophys. J. 89*, 3129–3140.

94. Janovjak, H., Sapra, K. T., Kedrov, A., and Muller, D. J. (2008) From Valleys to Ridges: Exploring the Dynamic Energy Landscape of Single Membrane Proteins. *ChemPhysChem 9*, 954–966.
95. Janovjak, H., Struckmeier, J., Hubain, M., Kedrov, A., Kessler, M., and Muller, D. J. (2004) Probing the energy landscape of the membrane protein bacteriorhodopsin. *Structure 12*, 871–879.
96. Engelman, D. M., Chen, Y., Chin, C. N., Curran, A. R., Dixon, A. M., Dupuy, A. D., Lee, A. S., Lehnert, U., Matthews, E. E., Reshetnyak, Y. K., Senes, A., and Popot, J. L. (2003) Membrane protein folding: Beyond the two stage model. *FEBS Lett. 555*, 122–125.
97. Janovjak, H., Knaus, H., and Muller, D. J. (2007) Transmembrane helices have rough energy surfaces. *J. Am. Chem. Soc. 129*, 246–247.
98. Sanders, C. R., and Myers, J. K. (2004) Disease-related misassembly of membrane proteins. *Annu. Rev. Biophys. Biomol. Struct. 33*, 25–51.
99. Hunte, C., Screpanti, E., Venturi, M., Rimon, A., Padan, E., and Michel, H. (2005) Structure of a Na^+/H^+ antiporter and insights into mechanism of action and regulation by pH. *Nature 435*, 1197–1202.
100. Kedrov, A., Appel, M., Baumann, H., Ziegler, C., and Muller, D. J. (2008) Examining the dynamic energy landscape of an antiporter upon inhibitor binding. *J. Mol. Biol. 375*, 1258–1266.

BI800753X